CLM-P 109

United Kingdom Atomic Energy Authority

RESEARCH GROUP

Preprint

THE ULTRAVIOLET EMISSION SPECTRUM OF THE SOLAR CHROMOSPHERE AND CORONA

W. M. BURTON
A. RIDGELEY
R. WILSON

Culham Laboratory,

Culham, Abingdon, Berkshire

1966

THE ULTRAVIOLET EMISSION SPECTRUM OF THE SOLAR CHROMOSPHERE AND CORONA

by

W.M. BURTON
A. RIDGELEY
R. WILSON

(Submitted for publication in Mon. Not. Roy. Astron. Soc.)

A B S T R A C T

A stabilised Skylark rocket flown on 9th April, 1965 provided observations of the emission spectrum of the solar chromosphere and corona. Servo-controlled alignment systems stabilised an image of the sun with an accuracy of a few seconds of arc relative to the spectrograph slit which was set at about 10 arcsec outside the solar limb. The ultraviolet spectrum between 950 Å and 2950 Å was recorded on photographic film at altitudes from 100 km to 160 km. About 300 emission lines were observed and a list of wavelengths with estimated intensities is given, together with identifications for about three-quarters of the observed lines. New identifications include intersystem transitions in CIII, NIV, OV and new forbidden transitions in FeXI and FeXII. The intensities of the chromospheric emission lines are compared with previous measurements obtained by direct observation of the solar disk.

U.K.A.E.A. Research Group,
Culham Laboratory,
Nr. Abingdon,
Berks.

July, 1966 (MEA)

C O N T E N T S

1. Introduction

The development of an attitude stabilisation system for the Skylark rocket has provided a vehicle from which solar observations can be carried out with good spatial resolution. Details of the stabilised Skylark vehicle[1] and of the experiments flown during the first two proving flights[2] have been reported previously. The third flight took place on 9th April 1965 at 01.00 U.T. from Woomera, South Australia and again carried instruments prepared by Culham Laboratory. The instrumentation was designed to provide two types of observation. First, the ultraviolet spectrum of the chromosphere and corona between 950 Å and 2950 Å was observed 10 arcsec outside of the solar limb, and secondly, spectroheliograms were obtained in emission lines of HeII 304 Å, FeIX-XII near 180 Å and in the 40-60 Å region. A brief description of the results obtained from this flight has already been published[3] and the purpose of this paper is to give a detailed account and analysis of the results obtained by the first of the two experiments.

A normal incidence spectrograph was used to record the spectrum from a region just outside the solar limb with spatial resolution adequate to separate the spectrum of the chromosphere and corona from that of the photosphere. The latter is very intense at wavelengths above about 1800 Å and in this region the problems are comparable with those encountered when making ground-based coronagraphic observations, but with the added complexity involved in a rocket experiment. The great advantage obtained is the removal of atmospheric scattering and absorption. The observed spectrum includes many emission lines which have not been observed previously because of the masking effect of the high background emission from the photosphere.

An analysis of the observed spectrum has provided a wavelength list of about three hundred emission lines together with estimated intensity data based on preliminary calibration measurements. About 75 per cent of the lines have now been identified and these include several transitions which have not previously been reported in the solar spectrum and also new lines not observed in the laboratory.

2. Instrumentation

The Skylark vehicle attitude stabilisation system provided a pointing accuracy of a few minutes of arc in the lateral axes using photoelectric sensors to give the required error signals. An accuracy of about five degrees was obtained in the roll axis using the earth's magnetic field for error sensing. The stabilisation provided by this primary

vehicle control system is not adequate to isolate the solar chromosphere from the photospheric background and a secondary alignment system was used. The servo-controlled optical alignment system was of similar type to that used on the two previous stabilised Skylark flights[2,4] but the gear driven mirror system was replaced by an electromagnetic actuator which was flown for the first time on this occasion. The servo-controlled primary mirror stabilised an image of the sun relative to the spectrograph slit with an accuracy of about three seconds of arc. The slit was set ten seconds of arc outside of the solar limb, in order to observe the spectrum of the chromosphere with minimum interference from the intense photospheric background. The slit width was 10 microns which is equivalent to 4 arcsec or 3000 km at the sun and therefore covered the entire transition zone between the chromosphere and inner corona[5].

A schematic diagram of the optical system is shown in Fig.1. The direction of the solar radiation is coincident with the stabilised roll axis of the vehicle. The primary concave mirror is 6 cm diameter and 50 cm focal length with an uncoated front surface of polished fused quartz. An image of the sun 4.7 mm diameter is formed by the mirror at the slit of the spectrograph. The grating is a Bausch and Lomb concave replica 40 cm radius, 1200 lines/mm used at normal incidence and blazed for optimum performance at about 2000 Å. A surface coating of aluminium with magnesium fluoride was selected to give maximum reflectance above 1200 Å. A six position camera provided a series of exposures on Kodak-Pathe SC5 and SC7 film. Each strip of film was curved to the 40 cm diameter Rowland circle and successive films were exposed by rotation of the camera drum according to a prearranged flight programme. At the end of the sequence a protective shutter closed and the films were subsequently removed from the rocket payload after parachute recovery. The flight on 9th April, 1965 provided six exposures of the solar limb spectrum between 950 Å and 2950 Å with a resolution of about 0.4 Å recorded at altitudes up to 160 km with exposure times between 3 seconds and 100 seconds.

One of the major problems associated with this experiment is the reduction of scattered light originating from the bright photosphere. The off-setting technique together with a suitable design of spectrograph is sufficient to reduce scatter of longer wavelength radiation ($\lambda > 3000$ Å) to a tolerable level. However, below 3000 Å the light scattered from the collector mirror is of the same wavelength as that being observed and no discrimination is possible within the spectrograph. The magnitude of this problem depends markedly on the wavelength observed, the photosphere being faint below 1800 Å and becoming intense at longer wavelengths. Between 1800 Å and 3000 Å the spectrum of the region just above the

solar limb cannot be observed unless the intensity of photospheric stray light scattered from the primary mirror is reduced to a level comparable with the intensity of chromospheric emission lines.

In a previous flight on 17th December 1964, the recorded spectrum was produced mainly by light scattered from the collector mirror and was consequently representative of the total sun. On that occasion a mirror coating of aluminium and magnesium fluoride was used to provide optimum reflectance above 1200 Å. During the pre-launch alignment tests at Woomera the optical system was tested in sunlight. The consequent exposure of the collector mirror surface in a dusty environment resulted in a slight deposition of dust which could not be completely removed before flight. Hence the careful precautions normally taken in coronagraphic work, where the optics are maintained in a clean environment throughout, were not possible. In the April 1965 flight this problem was solved by using an uncoated fused quartz collector mirror which could be carefully cleaned after the preparation tests and immediately prior to the assembly of the instrumentation on the rocket vehicle.

3. Results

An enlarged print of the solar limb spectrum between 950 Å and 2250 Å is shown in Fig.2. This was recorded on SC5 film during a 100 second exposure at a mean altitude of 155 km. The spectrograph slit was set tangentially about ten seconds of arc outside of the limb at the west equator of the sun, so that chromospheric radiation was focussed onto the centre point of the 8 mm length slit. Astigmatism in the concave grating spectrograph increased the length of spectral lines originating from this central slit point to about 0.5 mm at 1000 Å and about 3.5 mm at 3000 Å. The observed central strip of the spectrum has the form expected of the astigmatic spectrum formed by a point source at the slit centre and has its origin in the solar chromosphere.

The secondary spectrum recorded along the outer borders of the film results from solar radiation which has entered the full length of the spectrograph slit after being scattered from the surface of the primary concave mirror. It therefore represents the spectrum of integrated radiation from all parts of the sun and can be compared at any wavelength with the chromospheric spectrum recorded in the central strip of the film.

The chromospheric spectrum consists of many strong emission lines together with a fainter background continuum. Knowledge of the continuum intensity as a function of wavelength is of great importance for an understanding of the structure of the chromosphere

but the measurement is complicated by the uncertainty about the contribution of background scattering from the concave grating. Laboratory tests have shown that an intense visible light source at the centre of the slit can produce a scattered light pattern with the form of the observed central strip. The exact nature of this type of scattering is not fully understood at present and the present paper is confined to an analysis of the emission line spectrum. The investigation of a possible continuous spectrum component will be postponed until the necessary laboratory calibration work has been completed.

Wavelengths of emission lines were measured for the six films exposed during the flight. The position of lines were determined with an accuracy of about two microns using a measuring microscope and also a photoelectric spectrum plate measuring instrument[6]. Calculation of wavelengths was carried out by interpolation within 500 Å wavelength regions using a four coefficient polynomial determined by least-squares fitting of several selected standard lines in each region. The data reduction was carried out using a KDF9 computer system. The strongest emission lines were recorded on all six of the exposures and for these lines the wavelengths measured on six films are consistent to within 0.1 Å. The final measured wavelengths listed in Table 1 are based on mean values using all exposures which recorded a given line. Wavelengths of lines recorded on at least four films are expected to be accurate to ± 0.05 Å and these are marked 'a' in the table. The remaining unmarked lines were recorded on less than four films or were diffuse or blended lines which are less easily measured. In these cases the wavelengths are probably reliable to within ± 0.15 Å although the wavelength accuracy of many lines is considerably better than this figure. Wide or diffuse lines are marked 'w' in the table. Wavelengths below 2000 Å are vacuum values and above 2000 Å wavelengths in air are recorded.

The emission line intensities were estimated from microdensitometer scans of selected spectra. Characteristic curves (density-log intensity) for the photographic film were obtained from spectra recorded in a special calibration spectrograph. A calibration step filter of evaporated rhodium on quartz was used to produce fixed intensity levels at wavelengths of emission lines from a mercury vapour lamp. Characteristic curves measured at 1950 Å and 2537 Å were quite similar, indicating only a small dependence on wavelength. The characteristic curve measured at 1950 Å was used for the analysis of most of the flight films but the 2537 Å data was also used in estimating intensities of lines above 2500 Å. The films used to determine the calibration factors were taken from the same batch as the flight films and were processed under similar conditions, so that the calibration data could be used for the solar spectrum analysis. The absolute sensitivity of the flight

film was estimated by laboratory comparison with a sample of Kodak SWR film which had been previously calibrated to determine its sensitivity at 1216 Å. This calibration was based on a comparison measurement with a nitric oxide ionization chamber with a known sensitivity at 1216 Å, and was made using a source of monochromatic hydrogen Lyman-α radiation[7]. The response of SC5 emulsion at various wavelengths has been measured by Fowler et al[8] and for a particular photographic density their results indicate a uniform quantum response over the range 1000 Å - 3000 Å. This result was applied to the present data in order to extrapolate the 1216 Å calibration to other wavelengths. The overall instrument transmission was estimated before the flight by separate laboratory measurements of the primary mirror reflectivity and grating efficiency at various wavelengths between 1000 Å and 3000 Å.

Using these different calibration factors it was possible to convert the measured photographic densities into estimates of the energy flux in each emission line produced by the observed region of the solar chromosphere. No correction was made for atmospheric absorption in estimating the line intensities. Most of the intensity measurements were taken from exposures recorded at altitudes above 150 km. At this height the correction for residual atmospheric absorption is less than ten per cent for most wavelengths observed, so that the correction is small relative to the other uncertainties in the measurement.

Relative intensities should be quite reliable within restricted wavelength regions below 1900 Å where the probable error may be as low as ± 20%. However, the indirect calibration procedures described above cannot provide accurate absolute intensity data and the final estimated line intensities given in the table could be in error by a considerable factor. The probable error will be smallest for lines in the wavelength region 1200-1800 Å but beyond these limits the accuracy is reduced considerably. The large background corrections required at longer wavelengths introduce further errors and the intensities of lines above 2100 Å are bracketed to stress the low accuracy of the data.

Subject to these comments, the intensity values are given in the table are in units of 10^{-8} erg cm^{-2} sec^{-1} measured above the earth's atmosphere as emitted from the observed region at the solar limb.

4. Line Identifications

A list of the observed emission lines is given in Table I. The identifications are mainly taken from the NBS Ultraviolet Multiplet Table by C.E. Moore[9] where the transition details can be found by means of the multiplet numbers given in brackets following each

identification. A few lines were identified using the wavelength list compiled by Kelly[10] and these are denoted by (K) in the table. New identifications are denoted by a star in the third column of the wavelength list and the transition details are given for these lines. The observed spectrum is in good general agreement with published solar spectra reviewed by Tousey[11] but there are many important differences. The emission line intensities are considerably enhanced relative to the photospheric continuum and this has made it possible to detect new emission lines at wavelengths between 1900 Å and 2900 Å. Lines formed by highly ionized atoms also show enhancement relative to low ionization species because of the selection involved in the limb separation technique used in the Culham observations.

In addition to the many permitted lines the new spectra also show several intersystem transitions from metastable levels, which have enhanced relative intensity at the low electron density ($N_e \simeq 10^9$ cm^{-3}) existing in the solar chromosphere. Transitions of this type have been listed by Osterbrock[12] as predicted emission lines in the ultraviolet spectrum of gaseous nebulae and several of these lines are observed in the new chromospheric spectrum.

The configuration $1s^2\ 2s^2$ of the beryllium isoelectronic sequence give rise to separate singlet and triplet term systems. The intersystem transition ($2s\ ^1S_0 - 2p\ ^3P_1$) is not permitted in LS-coupling and has not been observed in the laboratory. In FVI some intersystem transitions have been observed, but for the other ions in this sequence the only estimates of the interval between the singlet and triplet ground states have been made by extrapolation and the accuracy is low. More accurate data is available in the case of CIII where the high level terms $6h\ ^1H$ and $6h\ ^3H$ can be used to connect the two systems[13].

The predicted CIII intersystem wavelength is 1908.73 Å which is in good agreement with a strong line observed at 1908.74 Å in the chromospheric emission spectrum. This line has not been reported in laboratory spectra and the only previous observation[14] appears to be in the spectrum of a quasar where the 1909 Å emission is red-shifted to an apparent wavelength of about 3900 Å. The wavelength of the corresponding intersystem transitions in NIV and OV can be estimated with an accuracy of about 3 Å by extrapolation, and otherwise unidentified lines are observed close to the predicted wavelengths. The suggested identifications are NIV (1486.57 Å) and OV (1218.30 Å) which locates the $2p\ ^3P_1$ level relative to the $2s\ ^1S_0$ ground state as 67,269 cm^{-1} in NIV and 82,082 cm^{-1} in OV. Continued extrapolation predicts the wavelength of this intersystem line in other ions of high solar abundance

as follows - NeVII (895 Å) MgIX (706 Å), AlX (638 Å) and SiXI (583 Å). The strong line at 1892.03 Å is the corresponding intersystem transition in SiIII which has a similar external configuration to the BeI sequence discussed above.

The Boron isoelectronic sequence forms separate doublet and quartet term systems so that the intersystem multiplet ($2s^2p\ ^2P - 2sp^2\ ^4P$) is a possible transition. The multiplet should occur at 2326 Å in CII but no positive identification can be made in the present spectra, probably because of the high background continuum level in this wavelength region. Several lines are observed in the solar spectrum between 1746 Å and 1754 Å close to the predicted NIII intersystem wavelengths. However, the presence in this region of strong FeII and NiII lines prevents any definite identification of the NIII multiplet. The OIV intersystem multiplet which has not previously been observed may be identified with a group of lines at 1399.83 Å, 1401.14 Å, 1404.80 Å and 1407.45 Å. These lines have the correct spacing and are within 5 Å of the predicted wavelengths. Assuming this identification, the $2p^2\ ^4P_{\frac{1}{2}}$ level can be located 71,437 cm^{-1} above the OIV ground state. A related ion with a similar outer electron configuration is SiII and the doublet-quartet intersystem transition is again possible. The new chromospheric spectrum shows two strong emission lines at 2334.36 Å and 2350.23 Å which are identified as components of the intersystem multiplet ($3s^2p\ ^2P - 3sp^2\ ^4P$) in SiII. The line at 2350.23 Å is the ($1\frac{1}{2} - \frac{1}{2}$) transition and the second line is probably a blend formed by the two transitions ($\frac{1}{2} - \frac{1}{2}$) 2334.40 Å and ($1\frac{1}{2} - 2\frac{1}{2}$) 2334.61 Å.

The carbon isoelectronic sequence has a ground state configuration $2p^2\ ^3P_0$ which can form singlet, triplet and quintet terms. The CI spectrum is well represented but includes one line at 1993.62 Å which cannot be identified with certainty. The wavelength agrees with the intersystem transition ($2p^2\ ^1D_2 - 3s\ ^3P_1$). However, the $3s\ ^3P_1$ level is not metastable and the multiplet at 1657 Å results from the allowed transition from this level to the ground state. The high anomalous intensity of the intersystem line is difficult to explain since the other transitions appear to follow LS-coupling selection rules. Although the wavelength agreement is excellent, the CI identification is doubtful and the line should be regarded as still unidentified. The quintet-triplet intersystem lines are not observed in CI or NII but the solar spectrum includes two lines close to the predicted wavelengths of this transition in OIII. The lines at 1660.85 Å and 1666.13 Å have the correct spacing and are identified as the intersystem multiplet ($2p^2\ ^3P - 2p^3\ ^5S$) in OIII. From this suggested identification the level of the $2p^3\ ^5S_2$ term can be determined as 60,210 cm^{-1} above the OIII ground state. Intersystem transitions between quintet and triplet terms

also give rise to the most important lines in the spectrum of OI(1356 Å) and SI(1900 Å, 1473 Å).

The spectrum of SiI as recorded in these latest observations shows some unusual features. In the wavelength region 1590 Å - 1600 Å several lines are observed which appear to be complete multiplets in SiI corresponding to transitions from high levels (6d, 7d, 8s) to the ground state $3p^2\ ^3P_0$. The multiplets are listed in the table only as possible identifications in spite of the excellent wavelength agreement, because of the absence of the corresponding lower members of the series spectra. The transitions from lower levels would normally produce the strongest lines but in the present spectra the only observed lines originate from high levels within 0.4 volts of the series limit. Tousey[10] has discussed the importance of recombination (SiII → SiI) in the formation of solar limb continuum below 1520 Å and the enhancement of the observed SiI multiplets may be connected in some way with the recombination process.

The emission spectrum of FeII is particularly important in the solar chromosphere and more than a hundred observed FeII lines are listed in the wavelength table. Many of these lines are also observed in absorption in the solar disk spectrum.

Two of the observed lines are quite different in appearance from the remainder of the chromospheric spectrum. These lines at 1242.15 Å and 1349.57 Å show emission extending for several minutes of arc above the solar limb and are probably coronal in origin. Earlier spectra recorded by the NRL group and discussed by Friedman[15] have also indicated the coronal nature of these lines. The visible emission line spectrum of the corona is produced largely by forbidden transitions between terms in the ground state configurations of highly ionized iron atoms and a similar origin was therefore considered for these two short wavelength lines. At the coronal temperature FeXII is an important ionic species but transitions between low ground level terms in FeXII have not been previously observed. Extrapolation along the $3p^3$ phosphorus isoelectronic sequence indicates that the ^2P levels in FeXII should be about 75,000 cm^{-1} above the ^4S ground state so that the predicted wavelength for the two ($^4S - ^2P$) lines is about 1300 Å. Quantum mechanical calculations have been carried out by Cowan[16] to determine term levels for ionized iron and his results place the predicted wavelengths within 6 Å of the observed coronal lines. The observed separation between the lines is 107.4 Å which agrees well with the predicted spacing of 105 Å. This agreement together with the characteristic spatial distribution suggests that the lines at 1242.15 Å and 1349.57 Å can be identified as the transitions ($^4S_{1½} - ^2P_{1½}$) and ($^4S_{1½} - ^2P_{½}$) in FeXII.

Comparison of the new solar limb spectrum with the stigmatic solar disk spectra described by Tousey[11] provides further points of interest. In the region 1380-1500 Å shown in Fig.3 the Culham spectrum is placed against a copy of the NRL disk spectrum which is skewed because of the double dispersion technique used to reduce stray light. Most of the lines agree well on the two spectra but the strong line at 1425 Å in the disk spectrum is very weak in the limb spectrum while the line at 1446 Å which is just detectable at the limb in the NRL spectrum appears strongly in the new solar limb spectrum. This line must originate in the chromosphere or low corona and although intense is not definitely identified. A possible identification for this line is the transition $^3P_1 - {}^1S_0$ in FeXI. Calculated values of the $^1S_0$ term level range from 80,300 cm^{-1} to 83, 150 cm^{-1} giving a predicted wavelength of 1448 ± 30 Å for the $^3P_1 - {}^1S_0$ interval[16]. The calculated transition probability for this line is more than an order of magnitude greater than that of any other transition between terms in the ground configuration of FeXI which is an abundant ion in the solar corona. If the line at 1445.89 Å is identified as FeXI ($^3P_1 - {}^1S_0$) then the level of $^1S_0$ can be determined as 81,830 ± 5 cm^{-1}. This enables the wavelength of the transition ($^1D_2 - {}^1S_0$) to be predicted as 2268 Å which could provide a direct check on the $^1S_0$ level value. Unfortunately the high background intensity at 2200-2300 Å prevents detection of lines in this region and no direct check can be made.

The instrumental resolution obtained in the flight exposures was limited to about 0.4 Å so that detailed analysis of line profiles was not possible. However, the hydrogen Lyman alpha line was fairly well resolved in one brief exposure of the solar disk obtained during the acquisition period of the pointing system. On this film the line shows a slight separation into two peaks spaced by 0.4 Å while the total line half width is about 1 Å which is in agreement with previous observations[11] on the HLα profile. Unfortunately, the limb spectrograms were too dense in HLα to draw any conclusions about its profile in this case.

5. Line Intensities

Although the purpose of this particular experiment was simply to survey the chromospheric/coronal spectrum at a point outside the limb, some information on line intensities was also obtained. Intensities are listed in Table I and an absolute calibration factor is given in the text but, for the reasons given, this is necessarily somewhat crude. With the assumptions of radial symmetry and small optical depth, the intensity of a spectral

line observed from just above the atmosphere of the earth can be expressed as

$$I_{limb} = \frac{R_\odot}{2L^2} \int_{x_1}^{x_2} \int_{x_1}^{\infty} \varepsilon_r \, dr \, dx \qquad \text{erg cm}^{-2} \text{ sec}^{-1}$$

where $R_\odot$ is the solar radius, L the earth's distance from the sun, x_1 and x_2 projected heights of the slit jaws above the solar limb, and ε_r the volume emission coefficient of the particular spectral line. During flight, x_1 and x_2 are time varying quantities due to the inaccuracy of guiding control which was estimated as ± 2 arc sec (± 1500 km) from telemetry records. The values of x_1 and x_2 set up in the alignment procedure prior to launch were 8 and 12 arcsec respectively (5800 and 8700 km).

In principle, measurements of this type with varying values of x_1 will allow the structure of the emitting layers to be determined. Controlled variation of the slit position was not attempted on this flight and in any case presents a difficult technical problem. The simplest solution is to consider two slit settings, one off the limb and the other on the disk. Disk observations already exist and a comparison with these was carried out. The measurements used are those obtained photographically by the NRL group[17] who gave values of the absolute flux from the total sun for a number of lines common to the present work. By applying the appropriate geometric factor, these measurements were reduced to disk intensities which correspond to the slit width employed in the present work and a slit length equal to the solar radius, i.e.

$$I_{disc} = \frac{R_\odot}{4\pi L^2} \, (x_2 - x_1) \int_0^{\infty} \varepsilon_r \, dr \qquad \text{erg cm}^{-2} \text{ sec}^{-1}$$

The ratio of I_{limb} to I_{disk} thus obtained is plotted against the ionization potential for various ions in Fig.4. Where more than one spectral line is available for a particular ion, the average has been taken. The plot shows the ratio increasing with ionization potential as would be expected from a radially increasing temperature distribution. An interpretation of Fig.4 in terms of structure is not possible since it is derived from observations of the sun at two widely different times with different photometric techniques. However, it is valuable to consider Fig.4 with the aim of checking the experimental performance of the equipment. If the observed scatter is ascribed entirely to photometric errors and if these are assumed to be equal in the two systems, then an error of ± 30% results for the NRL and Culham observations. This represents an internal error and does not include any systematic error due to errors in the absolute calibration. These are certainly very much larger in the case of the Culham measurements which are in a very preliminary state as far as photometry goes.

Approximate solutions to the integrals in the above expressions can be derived following the method of Pottasch[18] who assumes that for each ion ε_r is zero except within a restricted range of temperature. From the structure derived by Pottasch[5], the ions observed in the present case will be emitted from regions which are small compared to the projected slit width. This allows a simple solution for the integrals and predicts that the observed ratio for ions with $x_i \simeq 100$ eV ($T \simeq 1.5 \times 10^5$ ^oK) should be about an order of magnitude higher than the value observed. This discrepancy could be explained by the combined effects of

(a) errors in absolute intensity calibration

(b) a difference in solar conditions in the two flights (the Culham measurements were made of a very quiet sun as can be seen from the extreme ultraviolet spectroheliograms, obtained on the same flight[3])

(c) breakdown of the symmetry assumption

(d) errors in the structure derived by Pottasch

(e) any bias error between the pre-flight setting of the slit and its actual average position during flight.

At the present time we are most concerned with the last effect and a reasonable estimated upper limit can be obtained by ascribing the full discrepancy to this case. This results in an error of 1.5 arcsec in the sense that the observed region was further away from the solar limb. It seems unlikely that the actual error was greater than this, a conclusion which is supported by the general trend of the results in Fig.4 which include low and neutral stages of ionization. The conclusion that the bias error is probably less than 1.5 arcsec is encouraging as far as the operation of the equipment is concerned but the analysis underlines the need for very accurate settings in future flights.

An estimate of the scatter coefficient of the collector mirror during flight can also be derived from the photometry of the observed spectra. The scattered light at HLα is apparent on several spectrograms and extends over the whole length of the slit. The absolute flux in this scattered image was estimated and compared to the total flux in HLα from the whole disk. This value is now reasonably well established[15] as 5.1 erg cm^{-2} sec^{-1} at the earth. The scatter coefficient S is defined as the equivalent reflectivity of the collector mirror which would produce the observed scattered intensity in a direct image. The measurement gives $S = 7 \times 10^{-5}$ which is about an order of magnitude worse than can be obtained in a coronagraph (ignoring sky scatter). To obtain a true figure of merit S should be compared with the reflectivity R which is about 10% at HLα. Thus $S/R = 7 \times 10^{-4}$

and this value is consistent with the observed scattered light background at the longer wavelengths.

6. Acknowledgements

The results analysed in this paper were obtained by the combined efforts of several groups. We are grateful for the help of our colleagues in Spectroscopy Division at Culham and for the co-operation of the groups at R.A.E. Farnborough and W.R.E. Salisbury, Australia.

7. References

1. COPE, P.E.G. 1964. J. Brit. Interpl. Soc., 19, 285.

2. BLACK, W.S., BOOKER, D., BURTON, W.M., JONES, B.B., SHENTON, D.B. and WILSON, R. 1965. Nature, 206, 654.

3. BURTON, W.M. and WILSON, R. 1965. Nature, 207, 61.

4. BLACK, W.S. and SHENTON, D.B. 1966. "Peaceful Uses of Automation in Outer Space", 152. Plenum Press, New York.

5. POTTASCH, S.R. 1964. Space Science Reviews, 3, 816.

6. BOVEY, L., DAVIS, H.M., LOCKWOOD, W.H. and RICHARDS, E.W.T. 1962. J. Photogr. Sci. 10, 227.

7. BRANCH, J.D. 1964. Culham Laboratory Unpublished Information.

8. FOWLER, W.K., RENSE, W.A. and SIMMONS, W.R. 1965. Appl. Optics, 4, 1965.

9. MOORE, C.E. 1950. "An Ultraviolet Multiplet Table" Circular No.488. National Bureau of Standards, Washington, D.C.

10. KELLY, R. 1959. "Vacuum Ultraviolet Emission Lines", UCRL Report No.5612.

11. TOUSEY, R. 1964. Quart. J. Roy. Astron. Soc., 5, 123.

12. OSTERBROCK, D.E. 1963. Planetary and Space Sci. 11, 621.

13. BOCKASTEN, K. Ark. Fysik., 1955. 9, 457.

14. SCHMIDT, M. Astrophys. J., 1965. 141, 1295.

15. FRIEDMAN, H. 1963. Ann. Rev. Astron. Astrophys., 1, 66.

16. COWAN, R.D. 1965. Private Communication.

17. DETWILER, C.R., GARRETT, D.L., PURCELL, J.D. and TOUSEY, R. 1961 Ann. Geophys., 17, 263.

18. POTTASCH, S.R. 1963. Astrophys. J., 137, 945.

TABLE I

Emission Line Wavelength List

Wavelength (Å)		Intensity	Identification			Comments
977.03	a	120	977.03	CIII	(1)	
1025.65		70	1025.72	HLβ	(2)	
1031.86	a	200	1031.91	OVI	(1)	
1037.62	a	100	1037.61	OVI	(1)	
1175.6	w	50	1175.6	CIII	(4)	Unresolved multiplet
1206.49		50	1206.51	SiIII	(2)	Blend with 1206.53 SiIII (11)
1215.58	w	6500	1215.67	HLα	(1)	
1218.30	a	20	*	OV		$(2s^2\ ^1S_0 - 2p\ ^3P_1)$
1238.81	a	30	1238.80	NV	(1)	
1242.15		25	*	FeXII		$(3p^3\ ^4S_{1\frac{1}{2}} - 3p^3\ ^2P_{1\frac{1}{2}})$
1242.79		15	1242.78	NV	(1)	
1264.75	a	20	1264.73	SiII	(4)	
1298.88	a	15	1298.89	SiIII	(4)	Blend with 1298.96 SiIII (4)
1300.84		10	1301.14	SiIII	(4)	
1302.15	a	30	1302.17	OI	(2)	
1303.10		10	1303.32	SiIII	(4)	
1304.78	a	30	1304.86	OI	(2)	
1305.91	a	20	1306.02	OI	(2)	
1309.25		20	1309.27	SiII	(3)	
1334.58	a	120	1334.52	CII	(1)	
1335.72	a	200	1335.68	CII	(1)	
1349.57	a	30	*	FeXII		$(3p^3\ ^4S_{1\frac{1}{2}} - 3p^3\ ^2P_{1\frac{1}{2}})$
1351.49		20				
1355.47		40	1355.61	OI	(1)	
1358.36		20	1358.52	OI	(1)	
1371.26		30	1371.29	OV	(7)	
1393.76	a	300	1393.76	SiIV	(1)	
1399.83		20	*	OIV		$(2p^2\ ^2P_{1\frac{1}{2}} - 2p^2\ ^4P_{1\frac{1}{2}})$
1401.14	a	60	*	OIV		$(2p\ 2P^2_{1\frac{1}{2}} - 2p^2\ 4P^2_{2\frac{1}{2}})$
1402.73	a	150	1402.77	SiIV	(1)	
1404.80	a	40	*	OIV		$(2p\ ^2P_{1\frac{1}{2}} - 2p^2\ ^4P_{1\frac{1}{2}})$
1406.05		20				
1407.45	a	20	*	OIV		$(2p\ ^2P_{1\frac{1}{2}} - 2p^2\ ^4P_{1\frac{1}{2}})$
1416.99		20				Possible 1416.97 SiII (18.06)
1424.85		20				Possible 1424.78 SiIII (62)
1440.37		20				
1445.89	a	40	*	FeXI		$(3p^4\ ^3P_1 - 3p^4\ ^1S_0)$
1454.90		20	1454.96	NiII	(7)	
1463.61		20	1463.48	NiII	(K)	
1467.36	a	40	1467.45	CI	(36)	
1472.97	a	40	1472.97	SI	(4)	
1474.05	w	20	1473.98	SI	(3)	
1481.58		30	1481.65	SI	(4)	
1483.01	w	10	1483.05	SI	(3)	
1486.57	a	40	*	NIV		$(2s^2\ ^1S_0 - 2p\ ^3P_1)$
1510.87	a	30	1510.86	NiII	(6)	
1526.71	a	60	1526.72	SiII	(2)	
1529.35		30				
1530.89	a	40				
1532.52	a	30	1532.56	PII	(1)	
1533.49	a	80	1533.45	SiII	(2)	
1534.52		40				
1537.22	a	60				
1540.87	w	50				
1541.34		40				
1541.94		30				
1542.20		20	1542.32	PII	(1)	
1543.84	a	30				

Wavelength (Å)		Intensity	Identification			Comments
1544.73		40				
1545.18		50				
1548.20	a	1500	1548.20	CIV	(1)	
1550.74	a	800	1550.77	CIV	(1)	
1551.89		60				
1555.57		30				
1558.87	a	100	1559.11	FeII	(45)	Blend with 1558.71 FeII (46)
1560.42		100	1560.31	CI	(3)	
1560.66		100	1560.70	CI	(3)	
1561.21		60	1561.40	CI	(3)	
1563.76	a	100	1563.79	FeII	(45)	
1566.80	a	60	1566.83	FeII	(44)	
1567.95		40	1568.03	FeII	(45)	
1569.70		60	1569.67	FeII	(44)	
1570.19		80	1570.25	FeII	(45)	
1571.29		50				
1572.72		10	1572.75	FeII	(45)	
1573.76	a	80	1573.83	FeII	(45)	
1574.85	a	120	1574.93	FeII	(45)	Blend with 1574.78 FeII (44)
1576.98	a	60	1577.16	FeII	(45)	
1578.33		40				
1580.57	a	80	1580.64	FeII	(44)	
1584.93	a	80	1584.95	FeII	(44)	
1588.28	a	80	1588.30	FeII	(44)	
1590.49		20				Possible 1590.49 SiI (36)
1592.30		40				Possible 1592.35 SiI (36)
1594.62	a	50				Possible 1594.53 SiI (36)
1595.07		40				Possible 1594.92 SiI (34)
1595.58		10				Possible 1595.50 SiI (34)
1597.93		10				Possible 1597.99 SiI (34,35)
1600.09		20				
1600.99		20				
1602.43	a	60				
1603.28		50				
1605.47		20	1605.57	NiII	(K)	
1606.84		20				
1608.48	a	50	1608.45	FeII	(8)	
1610.98	a	100	1610.93	FeII	(43)	
1612.82	a	120	1612.81	FeII	(43)	
1614.45	a	50				Possible 1614.55 SiI (30)
1616.57		40				Possible 1616.55 SiI (30)
1618.41	a	60	1618.46	FeII	(8)	
1621.63	a	50	1621.69	FeII	(8)	
1623.10	a	80	1623.10	FeII	(43)	
1625.56	a	120	1625.53	FeII	(43)	
1627.26	a	60				
1629.34	w	60	1629.16	FeII	(8)	Possible 1629.47 SiI (29) blend
1631.16	a	40	1631.12	FeII	(8)	
1632.61	a	80	1632.67	FeII	(43)	
1633.91	a	100	1633.91	FeII	(43)	
1635.48		10	1635.39	FeII	(68)	
1637.37	a	100	1637.40	FeII	(42)	
1640.36	a	500	1640.47	HeII	(12)	Blend with 1640.17 FeII (43)
1642.38		40				
1643.54	a	120	1643.59	FeII	(42)	
1644.97	a	40				
1647.40		20				
1649.37	a	80	1649.44	FeII	(42)	
1654.30	a	100	1654.48	FeII	(42)	
1656.33	a	150	1656.26	CI	(2)	
1657.06	a	200	1657.00	CI	(2)	
1657.39	a	200	1657.37	CI	(2)	
1657.86	a	200	1657.89	CI	(2)	
1658.58		150	1658.11	CI	(2)	Blend with 1658.79 FeII (41)

Wavelength (Å)		Intensity	Identification			Comments
1659.39	a	150	1659.49	FeII	(40)	
1660.85	a	120	*	OIII		$(2p^2\ ^3P_1 - 2p^3\ ^5S_2)$
1663.20	a	100	1663.23	FeII	(40)	
1666.13	a	220	*	OIII		$(2p^2\ ^3P_2 - {}^2p^3\ ^5S_2)$
1667.95		20				
1669.63	a	60				Possible 1669.67 AIII (6)
1670.82	a	250	1670.76	FeII	(40)	Blend with 1670.81 Al II (2)
1673.46	a	80	1673.47	FeII	(102)	Possible 1673.43 AIII (6) blend
1674.32	a	100	1674.26	FeII	(41)	
1674.58		80	1674.72	FeII	(40)	
1676.36		60				
1676.80		100	1676.87	FeII	(41)	
1679.36	a	80	1679.39	FeII	(102)	
1681.03	a	100				
1683.49		20				
1686.08		120	1685.95	FeII	(41)	
1686.45	a	150	1686.46	FeII	(40)	
1688.28	a	80				
1689.79	a	60	1689.82	FeII	(85)	
1690.82		20	1690.78	FeII	(85)	
1691.20	a	100	1691.29	FeII	(41)	
1692.53	a	60	1692.51	NiIII	(16)	
1693.83		60	1693.96	FeII	(41)	
1694.38	a	80				
1696.68	a	150	1696.80	FeII	(38)	
1698.08	a	60	1698.19	FeII	(40)	
1698.94		50				
1700.30	w	20				
1701.99	a	200	1702.05	FeII	(38)	
1703.36	a	80	1703.41	NiII	(5)	
1704.51	a	100	1704.67	NiII	(U)	
1706.06	a	100	1706.18	FeII	(38)	
1707.40	a	80	1707.41	FeII	(84)	
1708.52	a	150	1708.63	FeII	(38)	
1709.53	a	120	1709.60	NiII	(4)	Blend with 1709.68 FeII (84)
1711.48	a	20				
1713.01	a	250	1713.00	FeII	(38)	
1715.00		60	1715.04	FeII	(84)	
1715.54		120	1715.51	FeII	(84)	
1716.51	a	200	1716.57	FeII	(39)	
1717.84	a	120				
1718.60		20	1718.52	NIV	(7)	
1720.50	a	250	1720.62	FeII	(38)	
1722.38	a	80	1722.53	SiIV	(10)	
1724.79	a	250	1724.85	FeII	(39)	Blend with 1724.96 FeII (37)
1726.33	a	250	1726.39	FeII	(38)	
1727.37		20	1727.38	SiIV	(10)	
1728.84	a	100				
1731.02	a	150	1731.04	FeII	(110)	
1731.85		100				
1733.33		80	1733.33	FeII	(110)	Blend with 1733.13 NiIII (15)
1734.54		60				
1737.39	w	100				
1740.12	a	80				
1741.53	a	150	1741.56	NiII	(5)	
1746.78	a	80	1746.82	FeII	(101)	
1747.06		20	1747.01	NiIII	(15)	
1748.30	a	120	1748.30	NiII	(5)	
1749.56		80				Possible NIII $(2p\ ^2P_{1\frac{1}{2}} - 2p^2\ ^4P_{2\frac{1}{2}})$
1751.84	a	150	1751.92	NiII	(4)	
1754.12	a	60				Possible NIII $(2p\ ^2P_{1\frac{1}{2}} - 2p^2\ ^4P_{1\frac{1}{2}})$
1754.72	a	100	1754.81	NiII	(4)	
1759.72	a	60				
1761.30	a	120	1761.38	FeII	(101)	

Wavelength (Å)		Intensity	Identification			Comments
1763.97	a	60				
1765.54	a	80				
1766.36		50				
1769.66		60	1769.64	NiIII	(14)	
1772.48	a	150	1772.52	FeII	(99)	
1773.85	a	80	1773.96	NiII	(3)	
1776.34		30				
1781.29	a	50	1781.28	NiIII	(K)	
1788.29	a	100	1788.50	NiII	(5)	
1793.28	a	60	1793.37	FeII	(99)	
1798.11	a	80	1798.16	FeII	(142)	
1804.52		5	1804.48	NiII	(2)	
1807.94	a	1500	1808.00	SiII	(1)	Blend with 1807.31 SI (2)
1809.29		60	1809.32	FeII	(142)	
1817.02	a	2500	1816.92	SiII	(1)	
1817.49		1000	1817.46	SiII	(1)	
1818.62		80	1818.51	FeII	(66)	
1820.19	a	60	1820.37	SI	(2)	
1821.99	a	100	1822.15	FeII	(66)	
1823.90	a	100	1323.89	FeII	(K)	
1326.16		80	1826.25	SI	(2)	
1826.83		60	1826.99	FeII	(65)	
1828.93		50				
1831.72		100	1831.72	FeII	(66)	
1832.84		50	1832.68	NiII	(2)	Blend with 1833.07 FeII (66)
1835.74		100	1835.87	FeII	(98)	
1839.16		50				
1841.63	a	120	1841.70	FeII	(65)	
1842.97		60				
1844.82	a	50				
1846.56	a	80	1846.58	FeII	(98)	
1847.88		40				
1848.77	a	30	1848.77	FeII	(141)	
1849.82		10				
1851.62	a	60	1851.62	FeII	(65)	
1854.77	a	220	1854.72	AlIII	(1)	
1859.92	a	300	1860.04	FeII	(97)	Blend with 1859.74 FeII (65)
1862.78	a	150	1362.78	Al III	(1)	
1864.67	a	120	1864.74	FeII	(126)	Blend with 1864.66 FeII (126)
1876.86	a	180	1876.84	FeII	(97)	
1877.55		40	1877.46	FeII	(125)	
1880.05		40	1880.05	FeII	(141)	
1880.96	a	120	1880.98	FeII	(126)	
1888.03		150				
1892.05		1800	1892.03	SiIII	(1)	
1894.15		30	1894.00	FeII	(125)	
1895.57	w	30	1895.68	FeII	(124)	Possible blend 1895.46 FeIII (34)
1900.25	a	400	1900.27	SI	(1)	
1901.74	a	150				
1902.94		60				
1904.77		80	1904.78	FeII	(139)	
1908.74	a	600	1908.73	CIII	*	($2s^2\ ^1S_o$ - $2p\ ^3P_1$)
1910.62		50	1910.67	FeII	(124)	
1914.72	a	250	1914.68	SI	(1)	
1915.75	a	150				
1921.21		50				
1923.08		80				Possible 1923.01 CIII (K)
1926.08	a	220	1925.99	FeII	(123)	Possible blend 1926.30 FeIII (34)
1928.85		100				
1930.93	a	120	1930.93	CI	(33)	
1932.53	a	40	1932.48	FeII	(139)	
1935.24	a	120	1935.30	FeII	(96)	
1936.75	a	150	1936.78	FeII	(96)	
1993.62	a	1000				Possible 1993.65 CI (32)
2007.33	w	150	2007.45	FeII	(83)	

Wavelength (Å)	Intensity	Identification	Comments
2015.61	180	2015.50 FeII (83)	
2018.77	500	2018.77 FeII (94)	
2020.71	250	2020.74 FeII (83)	
2029.20	180	2029.18 FeII (93)	
2032.64	600	2032.41 FeII (94)	
2036.33	400	2036.44 FeII (137)	
2040.76	1500	2040.69 FeII (93)	
2051.10	800	2051.03 FeII (93)	
2055.57	600	2055.59 CrII (1)	
2057.30	400	2057.33 FeII (82)	
2061.66	700	2061.54 CrII (1)	
2063.65	800	2063.67 FeII (92)	
2065.44	300	2065.46 CrII (1)	
2068.06	500	2067.92 FeII (137)	
2080.39	800	2080.25 FeII (92)	
2083.4	800		
2334.4	(5000)	2334.40 SiII (0.01)	($3p\ ^2P_{1/2} - 3p^2\ ^4P_{1/2}$) } blend
		2334.61 SiII (0.01)	($3p\ ^2P_{1\,1/2} - 3p^2\ ^4P_{2\,1/2}$) } blend
2347.0	(1000)		
2348.2	(1000)	2348.10 FeII (36)	
2350.2	(3000)	2350.17 SiII (0.01)	($3p\ ^2P_{1\,1/2} - 3p^2\ ^4P_{1/2}$)
2359.9	(1000)	2360.00 FeII (3)	
2361.8	(1000)	2362.01 FeII (36)	
2375.0	(1000)	2375.19 FeII (36)	
2380.6	(1000)	2380.76 FeII (3)	
2381.9	(1000)	2382.04 FeII (2)	
2382.9	(1000)	2383.24 FeII (36)	
2468.4	(1000)	2468.30 FeII (113)	
2777.4	(1000)		
2795.6	(20000)	2795.52 MgII (1)	
2802.9	(10000)	2802.70 MgII (1)	

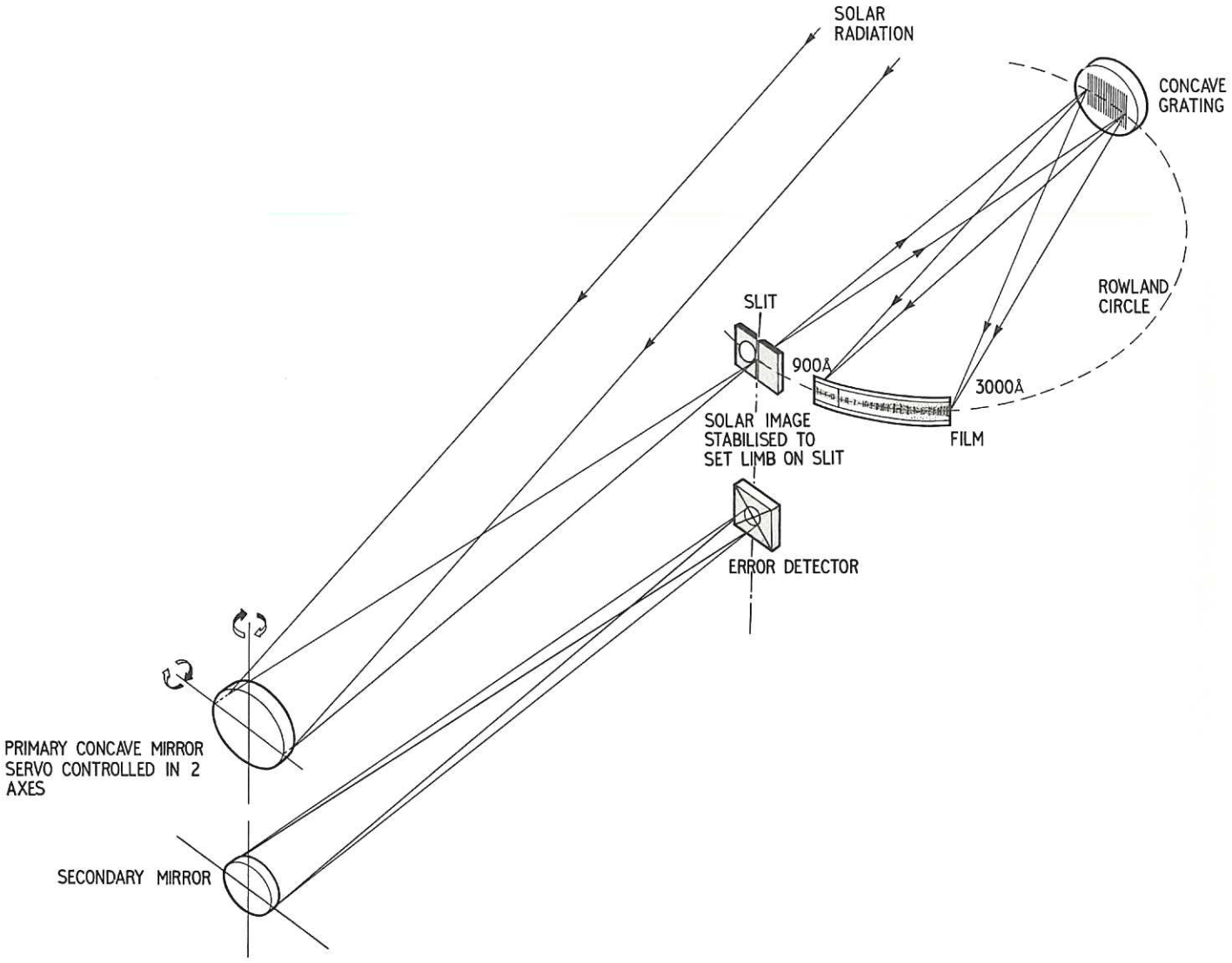

Fig. 1 Diagram of flight optical system (CLM-P 109)

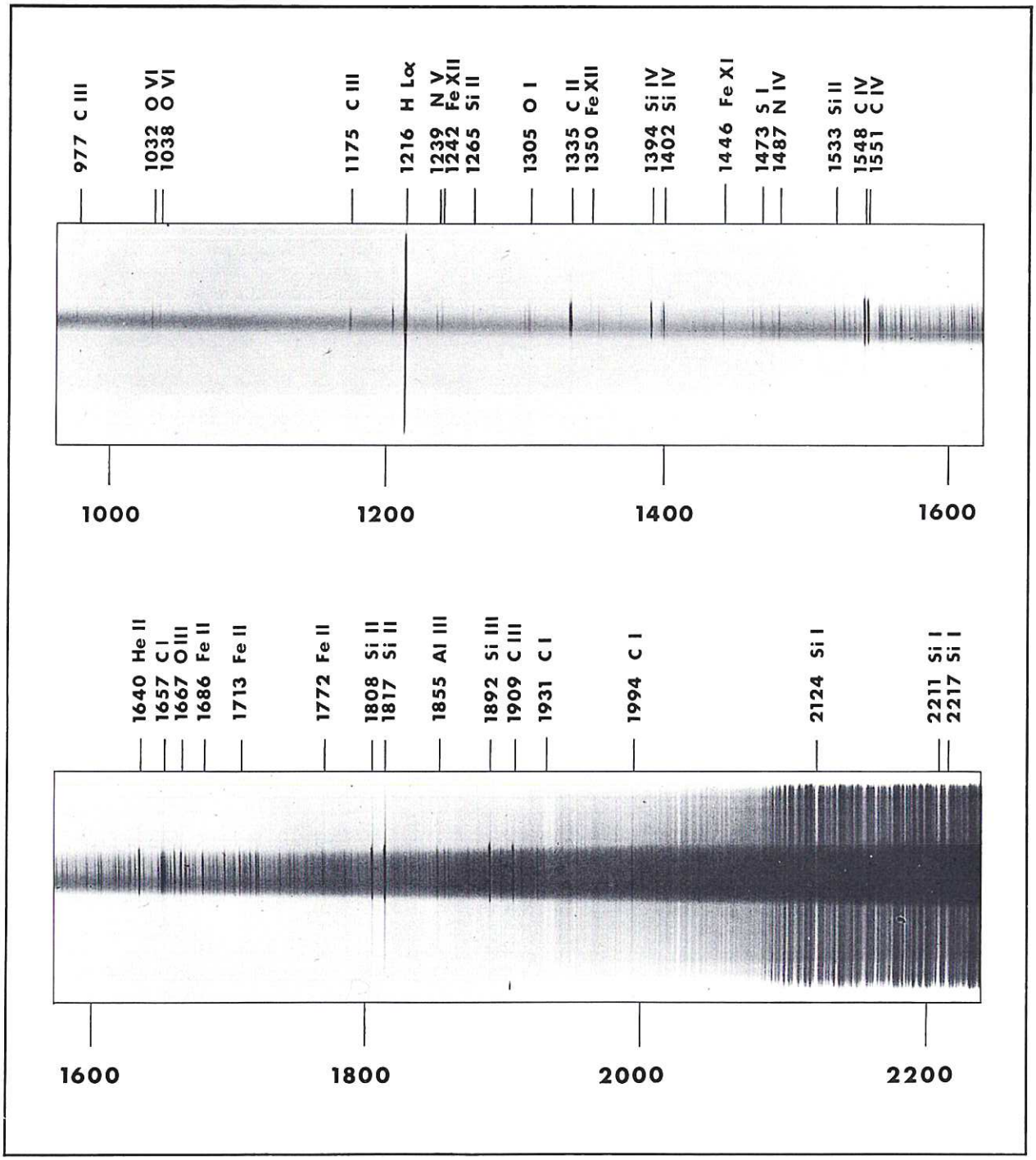

Fig. 2 Solar limb spectrum (950 Å - 2250 Å) (CLM - P 109)

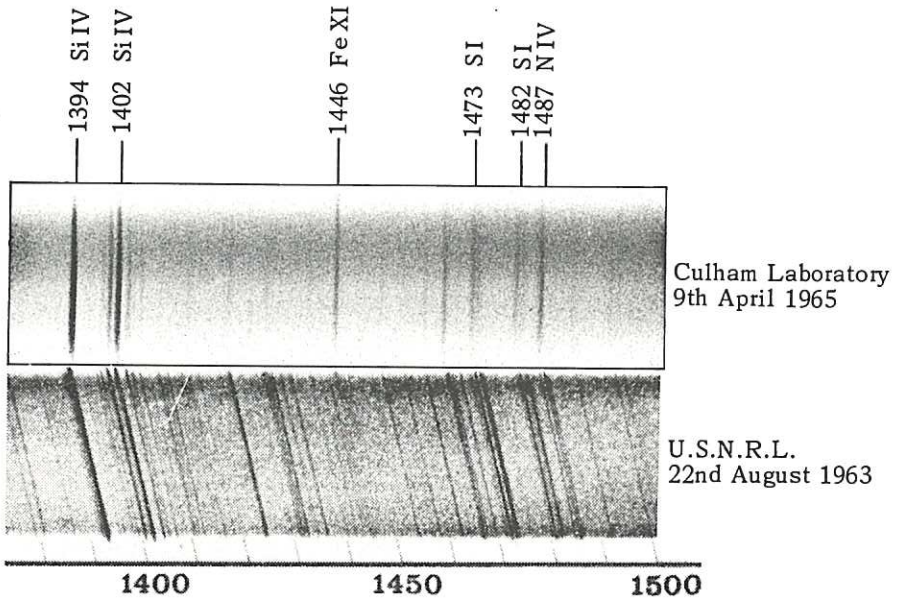

Fig. 3 Comparison of Culham and USNRL spectra (1380 Å - 1500 Å) (CLM-P 109)

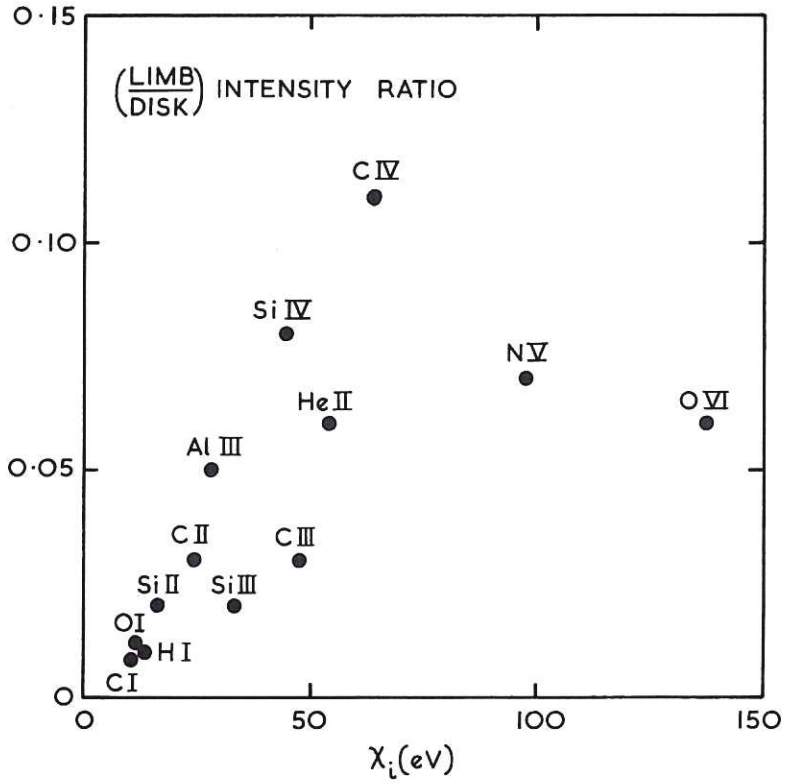

Fig. 4 (CLM-P 109)

The ratio of limb to disk intensities, derived from the present results and previous NRL observations respectively, plotted against ionization potential of each ion